Forest Ecology and Management 496 (2021) 119435

Contents lists available at ScienceDirect

Forest Ecology and Management

journal homepage: www.elsevier.com/locate/foreco

# Partitioning carbon losses from fire combustion in a montane Valley, Alberta Canada

S. Gerrand [a], J. Aspinall [a], T. Jensen [a,b], C. Hopkinson [a], A. Collingwood [c], L. Chasmer [a,*]

[a] Dept. of Geography and Environment, University of Lethbridge, Lethbridge, AB T1K 3M4, Canada
[b] Down to Earth Labs, 3510 - 6th Ave N, Lethbridge, AB T1H 5C3, Canada
[c] Parks Canada, 1 Compound Road, Waterton Park, AB T0K 2M0, Canada

ARTICLE INFO

*Keywords:*
Biomass
Soil carbon
Multi-spectral lidar
Fire severity
Carbon stocks
Remote sensing

ABSTRACT

Direct carbon (C) emissions from wildland fires have been difficult to quantify, especially in montane environments where sites are difficult to access. Here we examined pre-fire C partitioning and losses in a southern Canadian montane valley ecosystem, in Waterton Lakes National Park, Alberta Canada. The objectives of this study were to: (a) quantify the C loss due to combustion at a moist riparian site compared with a dry undulating upland site and (b) compare C loss observations to an active multi-spectral lidar remote sensing index.

C losses from wildfire were consistently greater at the wet riparian site compared with the dry valley site. Average soil C losses were 92.92 Mg C ha $^{-1}$ (st. dev. ± 48.60 Mg C ha $^{-1}$) and 58.05 Mg C ha $^{-1}$ (st. dev. ± 37.19 Mg C ha $^{-1}$). Average tree C losses were 114.0 Mg C ha $^{-1}$ (std.dev. ± 9.9 Mg C ha $^{-1}$) and 86.9 Mg C ha $^{-1}$ (std. dev. ± 13.5 Mg C ha $^{-1}$) respectively. C losses from trees were greater than soils, where trees lost 55% (moist riparian ecosystem) and about 60% (drier valley site) of C during combustion. Using post-fire multi-spectral airborne lidar data, we found that increased proportion of charred soils were significantly related to enhanced reflectivity in SWIR, resulted in more negative active normalised burn ratio (aNBR) results, indicating enhanced burn severity. Increased proportional cover of regenerating vegetation resulted in less negative aNBR both at the drier site, though no significant relationships between aNBR and charred vs. vegetated results were observed at the moist riparian site. No significant relationship was observed between depth of burn/soil C loss and aNBR derived from lidar data, indicating potential limitations when using burn indices for below canopy burn severity. The use of multi-spectral lidar may improve understanding of below canopy fire fuels and C losses in optical imagery, which often occludes these important components of fire ecology. The results of this research improve understanding of C losses associated with wildland fire in montane ecosystems that have undergone fire suppression and management by Euro-American colonizers for over 100 years.

## 1. Introduction

Temperate mountain ecosystems throughout western North America play a key role in partitioning carbon dioxide ($CO_2$) from atmospheric to terrestrial carbon (C) pools (IPCC, 2019). Old growth forests in the Pacific Northwest (Hudiburg et al., 2009) and similar forests in the Canadian/American Rocky Mountains (Bisbing et al., 2010) contain among the most C rich ecosystems on Earth (Law et al., 2018). For example, forests in the western United States (US) are estimated to account for 20–40% of the total US C sequestration (Huber et al., 2006; Pacala et al., 2001). Systematic disturbances to forested mountain ecosystems, such as droughts, forest clearing, and wildland fire, can result in mortality and C loss from these ecosystems (Zehetgruber et al., 2017; Bisbing et al., 2010). Despite this, montane forests continue to be significant terrestrial C sinks (Bartowitz et al., 2019) and are important for regional and global C budgets (Friedlingstein et al., 2019).

Cordilleran Montane forests provide significant fuel sources for combustion (tree canopies, understory, surface fuels, and combustible soils). The fuel conditions associated with higher elevations and a shortened fire season limit the ignition and spread of fire (Marcoux et al., 2015; Steel et al., 2015). In these moisture limited mountainous environments, fire frequency and the amount of biomass burned in each fire—otherwise referred to as fire severity (Keeley et al., 2009)—are loosely but inversely related: forests with low fire frequency can have

* Corresponding author.
*E-mail address:* laura.chasmer@uleth.ca (L. Chasmer).

https://doi.org/10.1016/j.foreco.2021.119435
Received 5 April 2021; Received in revised form 2 June 2021; Accepted 4 June 2021
Available online 12 June 2021

high losses of biomass in a single intense fire (Steel et al., 2015). Over longer periods, more frequent fires result in enhanced biomass loss from the ecosystem, such that total ecosystem C is reduced compared to an ecosystem with fewer fires (Bartowitz et al., 2019). As such, extreme weather events, and changing climate and hydrology are predicted to increase the frequency of fires in montane and subalpine forests (Westerling, 2016), possibly reducing the C storage capacity within these ecosystems (Law et al., 2003; Bisbing et al 2010; Bartowitz et al., 2019).

C losses from fire can be categorized in two ways: 1) initial loss of C from combustion, and 2) loss of C in the years following fire due to erosion, heterotrophic respiration, and reduced C uptake by vegetation compared with that prior to the fire (Irvine et al., 2007). While we can infer loss of biomass and C from above-ground forest vegetation, it is more difficult to determine the implications of the loss of C from soils due to burn severity (Bisbing et al., 2010; Zehetgruber et al., 2017; Hudak et al., 2020). Soil C may be a considerable proportion of total C in ecosystems that have deep organic soil layers. For example, the proportion of soil C in peatlands can be up to ~90% of total ecosystem C (van der Werf et al., 2010). In west coast, moist mountain ecosystems, Law et al. (2003) and Bisbing et al. (2010) suggest that soil C can account for ~50% of total ecosystem C. Incomplete quantification of C loss from large soil C pools has been a source of error in temporal estimations of post-disturbance ecosystem transition from C sources to C sinks. Partial accounting of belowground C losses can result in an underestimation of total C lost during a fire (Fellows et al., 2018). Further, understanding post-fire soil conditions, including amount of soil C remaining, also has important linkages to ecosystem recovery and may influence forest regeneration (Turner et al., 1999). Large organic matter losses from burned soils also influence soil biogeochemistry by altering pH, nitrogen (N) and C, potential exoenzyme activities, and can impact post-fire microbial communities (Whitman et al., 2019; Lybrand et al., 2018; Gongalsky & Persson, 2013). Organic matter loss has implications for seedbank recovery and the recruitment of coniferous saplings (Greene et al., 2007; Turner et al., 1999). Variation in some post-fire conditions caused by initial combustion of soil, such as altered C:N ratios, can affect the ability of forests to regenerate (Bartowitz et al., 2019), and forests can thus take different successional pathways that have long lasting implications on future C storage (Shenoy et al., 2011).

Despite the importance of soil C losses, measuring these losses is challenging (Boby et al., 2010; Fellows et al., 2018; Zhou et al., 2006). Field sampling often requires pre-fire measurements of soil quantities to determine spatial variations (Boby et al., 2010; Eisenberg et al., 2019). Other methods for identifying burn severity using remote sensing methods are often unable to consider ground cover and understory vegetation due to canopy occlusion of the burned surface (Chasmer et al., 2017, Gibson et al. 2020). Within montane ecosystems, valley sites can be highly productive and have high C storage capacity, yet quantification of the proportion of C lost from soils and the above-ground forest vegetation has significant uncertainties.

The overall objective of this research was to better understand the proportion of C lost from soils vs. above-ground forest vegetation due to combustion in dry vs. moist montane valley sites that have undergone 100 years of fire suppression and management by Euro-American colonizers in southern Alberta, Canada. Carbon loss was divided into i) C loss from soils; (ii) C losses that occurred during combustion from mature trees; and iii) C remaining in standing dead biomass (long-term losses, which will occur in the coming decades). To provide a framework for scaling the spatial variability of loss of C from trees and soils associated with scorching, we also compared loss of C to vegetation indices derived from airborne multispectral lidar data at the two sites. Results of this study have important implications for understanding climate change feedbacks and emissions modelling (Van der Werf et al., 2010; Friedlingstein et al., 2019), improving community and individual health risks from fire related smoke and aerosols (Langmann et al., 2009), understanding post-fire vegetative recovery (Irvine et al., 2007), and improving fire behaviour modelling (e.g. Hudak et al., 2020).

## 2. Materials and methods

### 2.1. Study area

This research was conducted in two study sites managed (and previously fire suppressed) by Euro-American colonizers: a moist forested montane riparian area (−114°2′19″W and 49°2′3″ N) and a nearby drier forested montane valley site (−114°2′26″W and 49°1′52″N). The sites are located in the Akamina Valley in Waterton Lakes National Park (WLNP) in the Canadian Rocky Mountains, Alberta Canada (Fig. 1). The mean annual air temperature of WLNP is 3.9 °C. Close proximity to the Rocky Mountain Continental Divide drives an orographically influenced moisture gradient, which decreases in average precipitation from west to east. On average, annual precipitation is 1520 mm near Cameron Lake (approximately 1 km from the sites) (Parks Canada, 2019). The pre-fire forests within this valley consisted of spruce species (*Picea* spp.) such as Engelman spruce (*Picea engelmannii*), white spruce (*Picea glauca*) and *P. englmannii* × *P. glauca* hybrids, as well as sub-alpine fir (*Abies lasiocarpa*), and lodgepole pine (*Pinus contorta*). Previous vegetation surveys from 2000 (available through Parks Canada) indicated low proportion of shrubs found in needle-leaved woodlands (between 5 and 10% coverage), likely due to high leaf area index and low light levels within similar valley forests. The stand was considered old growth/late successional as 20th century fire mitigation excluded the Akamina valley from wildfire disturbance in recorded history (at least but likely longer than 150 years). The moist riparian site (herein 'moist site') has an elevation of 1633 m, a slight sloping surface between 1.5 and 4.6º, and an average summer soil moisture of 13.8% (st. dev. ± 8.3%). The drier topographically variable upland valley site (herein 'drier' site) has an average elevation of 1654 m, a sloping surface between 4.2 and 9.8°, and an average summer soil moisture of 7.5% (st. dev. ± 3.4%). Soil moisture characteristics at the two sites were significantly different ($p = 0.0003$, T-test for unequal variance). The moist riparian site contains a combination of Humic Gleysol mineral soils and Fibrisol Organic soils of deep organic matter (≤150 cm) in poorly drained areas, and in depressions (Coen and Holland, 1976). The upland valley sites are dominated by Podzolic soils, which developed in glacial till (Coen and Holland, 1976).

The Kenow Wildfire was ignited by lightning ~10 km west of the Alberta-British Columbia border on August 30th 2017 (Kenow Fire Common Themes Analysis, 2018). On September 10-11th, 2017, high wind speed (max = 80 km/h, 5 day mean = 72 km/h), high temperatures (max = 26.5 °Cd, 5 day mean = 19.5 °C) and abnormally dry conditions (the third driest summer for this region on record), pushed the fire through the Akamina Valley. The high severity fire burned almost 100% of the forest canopy (Parks Canada, 2019) and approximately 35 000 ha, including 19 303 ha within WLNP. While North American wildland fires are often of mixed severity and leave behind landscape heterogeneity due to variations in successional age of the forest, topographic effects, and fuel structures (Turner et al., 1999; Marcoux et al., 2015; Perry et al., 2011), the Kenow fire burned unusually large, uniform patches at high severity (Eisenberg et al., 2019).

### 2.2. Field data collection

Field data were collected for this study from June 1st to September 30th in 2019 and 2020 at the moist site and July 15th to September 30th 2020 at the dry site within the montane Akamina Valley. To determine C content of soils and trees, we measured depth of burn using the adventitious roots method (Boby et al., 2010) and compared losses of soil C to collected soil cores from the nearby non-combusted areas. Tree mensuration plots were installed to determine biomass loss from combustion using allometry.

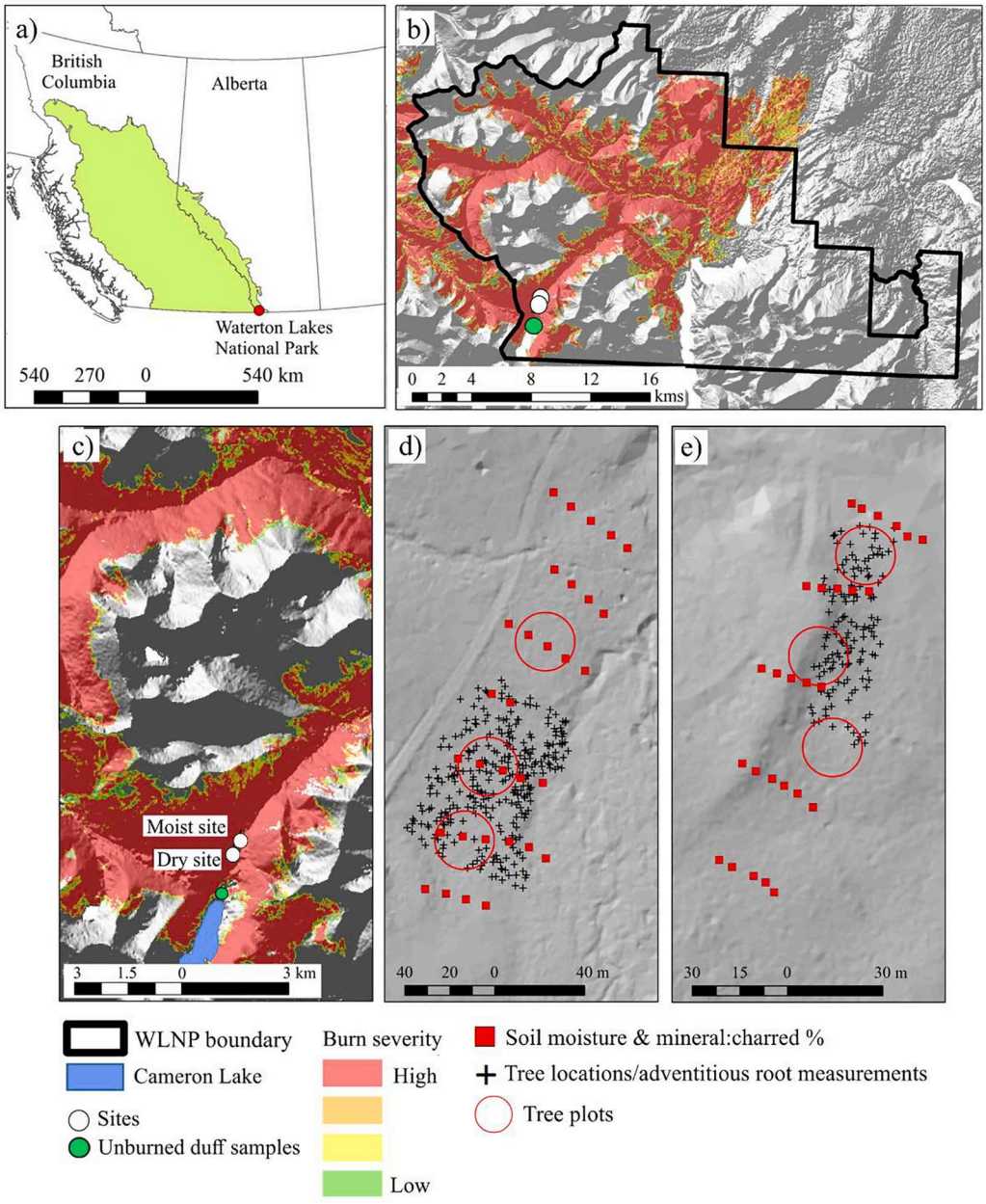


**Fig. 1.** a) Map of the location of Waterton Lakes National Park in the Montane Cordilleran ecozone in southern Alberta on the border of British Columbia and Montana; b) WLNP boundary, location of two main measurement sites with burn severity determined using difference normalised burn ratio (dNBR) from Landsat (provided by Parks Canada); c) illustrates the location of burned moist and dry sites as well as an unburned site used for measuring duff layer soil C, detail from b) including dNBR; d) moist site and e) dry site distribution of 1 m × 1 m plots (soil moisture and charred vs. mineral soil measurements), tree mensuration plots and tree locations for adventitious roots measurement. Circles representing tree mensuration plots are sized to scale.

*2.2.1. Aboveground tree measurements used to calculate biomass and C content*

All burned trees within three tree plots (11.3 m radius; 400 $m^2$) were measured at both sites and represent the characteristics and variability of the range of tree structures. Burnt 'spars,' or partially decayed trees, and trees <1.3 m within plots were excluded such that only live pre-fire tree biomass was considered. Each standing tree was numbered. Measurements included diameter at breast height (dbh), tree height, species, depth of burn (DOB) at the base of the tree bole (at each coordinate direction), and location using a differentially corrected Global Navigation Satellite System (GNSS) base station and rover with centimeter accuracy. Tree heights were obtained using a vertex hypsometer and dbh measurements were measured at a height of 1.3 m above ground level. Tree boles of fallen trees within each plot were also counted and measured (length and dbh at 1.3 m from root taper).

*2.2.2. Soil measurements*

Loss of organic soils during combustion was determined from depth of burn (DOB) measured using the adventitious root height method (Boby et al., 2010). The distribution of these roots following a fire often coincides with the pre-fire surface level when corrected for an adventitious root height (ARH) offset, which is the difference between ARH and the top of the green moss, or humus, in similar unburned forests (Boby et al., 2010). We sampled DOB within two years since the fire, which allowed us to observe scarring on the bark of trees where soil and mosses protected the bark of the tree from the intense heat of the flame front. Later, when the organic matter was reduced by smoldering combustion, or eroded, a clear line was left behind marking the pre-fire surface (Fig. 2).

We measured randomly sampled trees in a nearby unburned forest within 600 m of the dry site and 900 m of the moist site. The unburned site had the same tree species and similar environmental characteristics, also within the Akamina Valley. While this site remained unburned and could be considered a 'fire refugia' the vegetation characteristics do not match the characteristics of natural fire refugia described in Meigs and Krawchuk (2018) as the trees are large with a dense overstory canopy.


**Fig. 2.** Photographs of burn line scarring where lower portions of the tree bark are less heavily scorched due to protection of the now-burnt organic soils. Burn line scarring coincides with measured adventitious root height in a) right image and is offset by about 5 cm in b).

Areas with similar characteristics tend to burn most severely and are least likely to remain unburned. Therefore, we believe that the site remained unburned due to close proximity (within 100–200 m) to infrastructure, which was protected by air tanker and ground support. Unburned trees were used to determine an adventitious root height offset of 5 cm (st. dev. ± 4 cm, n = 10) specific to these sites. To accurately assess DOB in burned plots, we measured the burn line scarring and adventitious root heights in four cardinal directions (N, E, S, W) for each tree within burned moist (n = 313) and burned dry (n = 138) sites. The burn line scarring provides the most accurate measurement, but when this was not available, adventitious root height was used as an alternative. Measurements on four sides were averaged.

C content of the top 40 cm of soil cores were extracted from an unburned riparian forest duff layer (n = 10) in the same location as the unburned adventitious root offset measurements to capture a broad range of soil characteristics (Fig. 1c). Soil cores were located between trees to avoid contact with large tree roots and were a minimum of 10 m apart to minimize spatial autocorrelation of continuous soil horizons. In addition to these, 10 duff depth samples were measured with a 2 m probe proximal to soil cores to determine depth of peat. Soil cores were cut using a rectangular frame (7.5 cm × 7.5 cm) to a maximum depth of 40 cm and stratified into 10 cm sections for further analysis. Soil moisture content as wet volume ($V_w$) of each 10 cm section was determined and samples were placed in bags and sealed for laboratory analysis. Once in the lab, weights were measured and then the change in weight was determined from drying at 105 °C until the weight was non-varying.

#### 2.2.3. Plot measurements: volumetric water content and soil vs. vegetation proportions

Spatio-temporal variations in soil moisture within burned sites were determined by sampling within 31, 1 m × 1 m vegetation/moisture/charred plots established at the moist site, and 29 1 m × 1 m of the same plots established at the dry site (Fig. 1d, e). Soil moisture was measured biweekly in three locations within each 1 m plot with a Hydrosense soil moisture sensor (Campbell Scientific Inc.). Bi-weekly soil moisture data were collected at both sites four times between July 12th and August 5th, 2020. In the same 1 m × 1 m plots at both moist and dry sites, we also determined the proportion of charred (blackened soil) and proportion of mineral soils using red, green, blue (RGB) colour photography. Proportions of char and mineral were estimated visually as a percentage of each 1 m plot, where scorched black soil represent charred soils high in organic matter and grey/brown, rocky soils represent mineral soils with little to no organic matter remaining. Total soil proportion was determined by adding charred and mineral soils together. Areas within plots occluded by vegetation were excluded from classification.

#### 2.2.4. Locating plots and trees using kinematic global navigation satellite system

The location and elevation of tree mensuration plots, soil moisture plots, and individual trees corresponding with DOB measurements was determined using a Topcon Inc. (Canada) Hiper SR II survey-grade Global Navigation Satellite System (GNSS) with post-processing. Data were collected in kinematic and rapid static modes and corrected to a base station located within ~1.5 km from the sites. Surveyed measurement locations were at centimeter accuracy.

### 2.3. Remotely sensed data

#### 2.3.1. Multi-spectral lidar data collection

On July 16th, 2018, 10 months following the Kenow Wildfire, an airborne laser scanning (ALS) survey was conducted by the ARTeMiS Lab (University of Lethbridge). The system used was a Titan Multispectral Topo-Bathymetric Airborne Laser Scanner (Teledyne Optech Inc. Canada). Unlike most airborne lidar systems, the Titan has three laser channels (C1, C2, and C3) at wavelengths of 1550 nm (shortwave infrared; SWIR), 1064 nm (near infrared; NIR) and 532 nm (green), respectively (Hopkinson et al., 2016; Chasmer et al. 2017). The sensor was flown at a height of 1500 m above the valley floor. Each channel was set to operate at 125 kHz over a scanner field of view of 50°, which resulted in a total sampling rate of 375 kHz and about 10 laser pulse returns per $m^2$. At time of data collection, vegetation regeneration was minimal (moist site) to non-existent (drier site).

### 2.4. Data analysis

#### 2.4.1. Aboveground tree biomass calculations

To estimate biomass losses due to combustion and remaining post-fire scorched components on a per tree and per hectare (ha) basis, tree height and dbh measurements were input into species-based biomass equations described in Lambert et al. (2005) and Ung et al. (2008). Allometric models were used to partition biomass (and C content) within stem, branch, bark, and foliage biomass compartments as well as total aboveground biomass within each plot (Lambert et al., 2005). Shrubs were not included in the partitioning of C due to a) historically low shrub proportion (5% coverage, except for one site with 20% at 0.5–1 m height and 5–10% coverage at 2–5 m) found in valley forests identified by Parks Canada in 2000 (unpublished) and b) no indication or evidence that shrubs existed prior to fire in the burned study sites (no remaining shrub stems/root boles). Tree species were determined within plots based on tree structure, remaining cones and branch morphology. Unidentified tree species percent ranged from 2.9% (average within upland plots) to 29.3% (average within riparian plots). Unidentified trees were assigned an average biomass based on the proportional species distribution of successfully identified trees. For example, if a plot was 60% successfully identified as lodgepole pine, 60% of the unknown trees were assigned as Lodgepole pine for biomass calculation. To determine C content of biomass, we converted dry biomass to mass of C using species specific C concentration factors from Lamlom & Savidge (2003). This considers the range of C content in conifers between 47.21% and 55.2% depending on species (Lamlom & Savidge, 2003; Ma et al., 2020). C quantities and stem density per area of each plot were scaled to Mg/ha and stems/ha to describe landscape level stand structure.

#### 2.4.2. Soil carbon analysis

To determine soil C content within unburned duff cores, 10 cm sections were analysed individually to determine four key characteristics: volumetric water content (VWC), bulk density ($D_b$)—a ratio of dry solid mass to wet volume of soil and pores—,%C, and C content. Wet mass was recorded using a scale accurate to 1/100th of a gram before samples were dried in a forced air oven at 105 °C until mass stabilized to obtain dry mass. Bulk density ($D_b$) and volumetric water content (VWC) were then calculated as:

$$D_b = M_{dry}/V_{wet} \quad (1)$$

$$VWC = M_{wet} - M_{dry}/V_{wet} \quad (2)$$

where $D_b$ denotes bulk density, $M_x$ denotes mass at different times ($_x$), and $V_x$ denotes volume at different times ($_x$; Carter and Gregorich, 2010). For C analysis, organic matter of samples including small (<2cm diameter) roots were ground in a Wiley mill and reintroduced to the whole sample, which was screened with a 2 mm rolling screen. The 10 cm sample was then mechanically mixed and sub-sampled for combustion analysis so that percent of soil organic matter (SOM) and soil organic carbon (SOC) content from the subsample was representative of the entire 10 cm section. Percent SOM was calculated as [(pre-combustion mass minus post combustion mass) divided by pre-combustion mass] times 100 and C content is % C multiplied by bulk density:

$$\%SOM = [(M_{t1} - M_{t2})/M_{t1}]*100 \quad (3)$$

$$SOMloss = \%SOM*D_b \quad (4)$$

Samples were heated at 300 °C for 2 h and 600 °C for 5 h to ensure combustion of all organic matter for comparison of pre- and post-combustion mass. The van Bemmelen conversion factor of 1.724 from soil organic carbon to soil organic matter has been widely used in terrestrial and wetland soils (Wang et al., 2017). However, this is not a universal constant as the number can be influenced by factors such as vegetation cover, organic matter composition, depth in profile, and degree of decomposition, and when applied blindly can result in C overestimations of ~15% (Pribyl, 2010). In a critical review, Pribyl (2010) determined 1.9 as the median conversion factor among recent empirical studies. As such total dry SOM was then converted to SOC by dividing by the conversion factor of 1.9 to minimize these errors.

### 2.5. Geospatial data derivations

#### 2.5.1. Digital elevation model (DEM)

To determine continuous C losses from soils, we derived a 1 m interpolated DEM of the post-fire ground surface. To do this, we used a combination of C1 (1064 nm) and C2 (1550 nm) returns to increase data density and classified these into ground and non-ground returns in Terrascan (TerraSolid, Fl). Ground classified returns were interpolated in Surfer (Golden Software Surfer, CO, USA) using a triangulation with linear interpolation routine.

The DEM was then used to calculate a Topographic Position Index (TPI), which we assume to be a proxy for soil moisture. Areas of negative TPI values indicate locally topographic low-lying areas, or areas likely containing higher soil moisture, and positive TPI values indicate locally topographic hummocks or hills—areas of decreased soil moisture (Jenness 2006). TPI was calculated using Jenness (2006) using a search circular radius of 10 m, which was found to visually represent local undulations in topography. To determine slope variations between sites, the DEM was resampled to 5 m resolution and slope is calculated with the third-order finite difference method in ArcGIS Pro (ESRI, CA, USA).

#### 2.5.2. Estimating DOB and spatial distribution of soil C losses during combustion

To quantify soil C losses per site, the DEM was added to DOB measurements, allowing us to estimate elevation prior to fire. The sum of the DEM and DOB measurements were interpolated using a triangular irregular network (TIN) to model pre-fire elevation. The difference between the pre-fire DOB interpolation (TIN model) and the post-fire DEM were used to estimate depth of burn at 1 m spatial resolution. To quantify C losses from burned soils, C content within the soil samples collected from the unburned site near Cameron Lake were split into groups of lower (avg = 0.295% st.dev. ± 0.074%) and higher (avg = 0.599% st. dev. ± 0.165%) VWC, where groups are significantly different (*t*-test: $t_{24} = 4.85$, $p < 0.001$). Linear and exponential regression models were used to model the spatial distribution of C loss at riparian and upland burned sites based on topographic position and measured VWC. Loss of C from soil combustion was calculated as:

$$CumulativeC(kg/m^2) = Ccontent(kg/m)*depth(m) \quad (5)$$

per raster cell.

#### 2.5.3. Multi-spectral lidar-based active normalized burn ratio (aNBR)

To quantify the relationship between post-fire scorching of the ground surface and loss of C from soils (depth of burn), we use a multi-spectral lidar-based fire index (Chasmer et al. 2017), similar to that used when determining burn severity from optical imagery. This comparison provides quantification of the efficacy of optical imagery for C loss estimates from soils. Ground classified single laser return intensities for each channel were used along with returns to 0.3 m above the ground surface, such that undulations in slope were included. These were interpolated based on the average intensities within a 1 m search radius for localised comparisons with plot data (proportions of charred and mineral surfaces and early regeneration). These were used to calculate a lidar-derived active Normalized Burn Ratio (aNBR). aNBR is similar to optical remote sensing indices such as dNBR (e.g. Hall et al. 2008), where a normalized difference between NIR (1064 nm) and SWIR (1550 nm) wavelengths is calculated:

$$aNBR = NIR - SWIR/NIR + SWIR \quad (6)$$

While dNBR compares a Normalized Burn Ratio pre- and post-fire, aNBR has the advantage of obtaining spectral data from thematically classified point clouds, in this case, within the first year following wildland fire. The aNBR provides an advantage for detecting burn severity from features of interest (e.g., ground or canopy classified lidar returns) at fine spatial resolution (e.g., Chasmer et al., 2017). Because lidar is an active remote sensing technology, it is not influenced by the effects of shadows/occlusion, pre-/post-fire influences on phenology, and timing of data collection, which can increase variability of estimated burn severity in optical image ratios (e.g. Fraser et al. 2017; Chen et al. 2020).

### 2.6. Statistical comparisons

Differences between group means were compared by t-tests (for two groups) and one-way analysis of variance (ANOVA; for greater than two groups). Linear, exponential and polynomial regressions were used to assess correlations in continuous data.

## 3. Results

### 3.1. Soil C losses during combustion associated with depth of burn

Within the moist riparian site, we found that the Kenow fire burned deep into the duff and organic soil layers to the mineral soil to a mean depth of 18.2 cm (st. dev. ± 8.6 cm), with a maximum DOB of 52 cm found ~ 10 m away from a seasonal stream. The drier upland site experienced a shallower average depth of burn of 13.3 cm (st. dev. ± 6.7 cm), with a maximum DOB of 44 cm in a relatively flat at the base of a slope. This indicates that the accumulation of duff mosses within the riparian site was greater than that found at the drier upland site. In comparison, the depth of the duff layer to the mineral soil in four of 10 samples within the unburned forest near Cameron Lake (Fig. 1) were greater than 140 cm. The average depth of duff in the remaining six samples was 49 cm (st. dev. ± 27 cm). The long-term hydrology of the unburned forest provides explanation for the differences in moss accumulation between the two sites, especially where moist/saturated conditions likely reduced microbial decomposition of organic material. Post-fire soil moisture content of soil plots in the riparian site was 13.8% (average), associated with a near flat surface (mean slope up to 4°). In comparison, the drier upland site had a soil moisture of 8.1% (average) with a steeper mean slope up to 10°. Soil water accumulation in the riparian site likely increased moss productivity and reduced microbial decomposition in the period since the last fire (approximately 200 years ago; Harden et al., 1997). This may account for greater duff layer losses at the riparian site.

To quantify soil C loss from the depth of burn measurements, we applied soil C content equations [3–5] from unburned duff samples near Cameron Lake (Fig. 1). Within the unburned site, average bulk density per 10 cm section increases with depth ranging between 0.10 g/cm$^3$ (st. dev. ± 0.02 g/cm$^3$) at 0–10 cm to 0.13 g/cm$^3$ (st. dev. ± 0.01 g/cm$^3$) at 30–40 cm. Bulk density increases with depth due to compaction. Average bulk density of high VWC cores is 0.10 g/cm$^3$ (std. dev. ± 0.03 g/cm$^3$) and bulk density of low VWC is 0.17 g/cm$^3$ (std. dev ± 0.11 g/cm$^3$). Bulk density is significantly greater in cores with lower VWC (avg = 29.5% st.dev. ± 7.4%) compared with those that have higher VWC (avg = 59.9% st. dev. ± 16.5%, *t*-test:$t_{28} = -2.22$, $p < 0.05$).

Like bulk density, soil C content (Mg C ha$^{-1}$) increases with depth from surface and varies between moist and dry groups of samples. We found that soil C content is 456.2 Mg C ha$^{-1}$ (average; st. dev. ± 111.8 Mg C ha$^{-1}$) at 0–10 cm from the surface where samples were composed of undecomposed conifer needles, cones and living mosses. At deeper depths of 10–20 cm and 20–30 cm, soil C increases to 534.1 Mg C ha$^{-1}$ (st. dev. ± 95.5 Mg C ha$^{-1}$) and 571.59 Mg C ha$^{-1}$ (st. dev. ± 137.1 Mg C ha$^{-1}$), respectively due to decomposition and compaction—thus increasing the soil C content (Fig. 3) and reducing porosity. Average soil C content of high VWC cores is 433.8 Mg C ha$^{-1}$ (std. dev. ± 109.9 Mg C ha$^{-1}$) and soil C content of low VWC cores is 539.9 Mg C ha$^{-1}$ (std. dev. ± 105.4 Mg C ha$^{-1}$), indicating that soil C content is significantly greater within low VWC cores (*t*-test: $t_{25} = -2.67$, $p < 0.05$).

The relationship between depth and C content is explained using a linear function for dry cores ($n = 13$; $R^2 = 0.18$) and an exponential function for wet cores ($n = 17$; $R^2 = 0.32$) where C content for moist and dry soils is, respectively:

$$\mathrm{SoilC_{moist}} = 307.35e^{1.4622\mathrm{depth}} \quad (7)$$

and

$$\mathrm{SoilC_{dry}} = 533.43(\mathrm{depth}) + 441.06 \quad (8)$$

These equations provide a simple mechanism for estimating soil C losses at the site-level using the measured and lidar-derived difference elevation models and the local topographic position (TPI), where we assume that areas of low-lying elevation are closer to the water table and are therefore wetter (representing moist soil C (7)). Areas that are locally upraised, we assume, are further from the water table and are therefore drier (representing dry soil C (8)). These were partitioned at both sites and using depth of burn within those areas of low vs. high topographic features, equations (7) and (8) were applied based on measured interpolated depth of burn.

We found that the cumulative average loss of soil C from the riparian site was 92.9 Mg C ha$^{-1}$ (st. dev. ± 48.6 Mg C ha$^{-1}$), while maximum C loss of 341.8 Mg C ha$^{-1}$ was found approximately 10 m from a seasonal

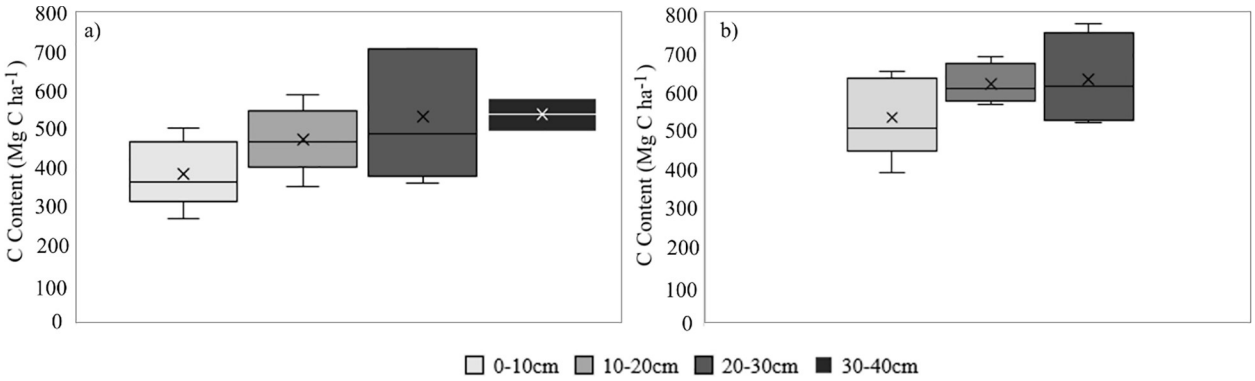


**Fig. 3.** Unburned peat samples are split into groups of higher (a) and lower (b) volumetric water content binned by depth. Both groups tend to show an increase in C density with increasing depth below the surface, with the drier group having slightly higher C content. Interquartile range is found at the upper and lower boundaries of each box (calculated with exclusive median), whiskers represent the maximum and minimum values outside of the third and first quartile, and mean and median are shown by the x and line within the box, respectively.

stream. The cumulative average loss of soil C from the upland site was 58.0 Mg C $ha^{-1}$ (st. dev. ± 37.2 Mg C $ha^{-1}$), with maximum losses of 213.6 Mg C $ha^{-1}$ found in a flat area at the base of a steeper slope (Fig. 4). Despite higher estimated C content in the upper layers of drier soils compared with moist soils, greater depth of burn in the riparian site resulted in greater overall losses of soil C. This is due in part to exponential increase in C content with depth at the riparian site, which resulted in an overall increased loss of soil C relative to the upland dry site.

### 3.2. C losses from combustion of tree canopies

Here we quantify the cumulative C losses from trees during combustion (instantaneous losses) and remaining partially burned standing and fallen tree stems within drier upland vs. moist riparian sites. Plots are partitioned into south, center, and north and run along the centre of the valley (Fig. 1d and e). Tree structures and C content of instantaneous loss components (foliage, bark) and partially burned longer-term C losses associated with tree fall and decomposition (stem and branches) within each plot are summarized in Table 1.

We found that total C losses from trees are 31% greater at the riparian site (avg = 114.03 Mg C $ha^{-1}$, ave. st.dev. ± 3.20 Mg C $ha^{-1}$) compared with trees found in the drier upland site (avg = 86.94 Mg C $ha^{-1}$, ave. st. dev. ± 1.01 Mg C $ha^{-1}$) (Table 1). Greater whole tree biomass losses at the riparian site were largely attributed to thicker stem diameters (dbh avg = 24.7 cm st. dev. ± 1.7 cm), despite shorter overall tree stature (avg = 15.73 m, st. dev. ± 8.50 m) and fewer trees (avg = 758 stems/ha). Upland sites, which have taller trees (avg = 17.62 m, st. dev. ± 3.32 m), and greater numbers of trees (avg = 983 stems/ha) also have narrower stems (dbh avg. = 19.9 cm, st. dev. ± 5.2 cm) (Table 1). While species distribution varies slightly between each plot within riparian and upland study areas, plots within the riparian site were dominated by white spruce and Engelmann spruce (74%), Lodgepole pine (21%), and sub-alpine fir (6%). The drier upland site was dominated by Lodgepole pine (60%), white spruce and Engelmann spruce (24%), and sub-alpine fir (17%). The propensity for large spruce trees in the riparian site indicates that these, in combination with higher water availability, are an important C storage species compared with higher density lodgepole pine in the drier upland site (Fig. 5).

When tree biomass was examined per species (Mg C $tree^{-1}$), rather than per area (Mg C $ha^{-1}$), the importance of spruce species (white and Engelmann) in moist riparian montane environments and the C losses associated with wildland fire is emphasized. There were no significant differences in Mg C $ha^{-1}$ lost between different species within the moist (ANOVA: $F_8 = 3.31$, $p > 0.05$) or dry sites (ANOVA: $F_{6=}3.24$, $p > 0.05$). However, the average Mg C $tree^{-1}$ lost during combustion from riparian site spruce trees is 0.15 Mg C $tree^{-1}$ (st.dev. ± 0.03 Mg C $tree^{-1}$) whereas average upland spruce lost 0.09 Mg C $tree^{-1}$ (st. dev. ± 0.02 Mg C $tree^{-1}$) – a difference of 38%, on average (Fig. 5). These drier valley/moist riparian differences in the amount of C lost from spruce trees during combustion are not significant in lodgepole pine (*t*-test: $t_3 = 2.46$, $p > 0.05$) or sub-alpine fir (*t*-test:$t_3 = 1.23$, $p > 0.05$) species (Fig. 5).

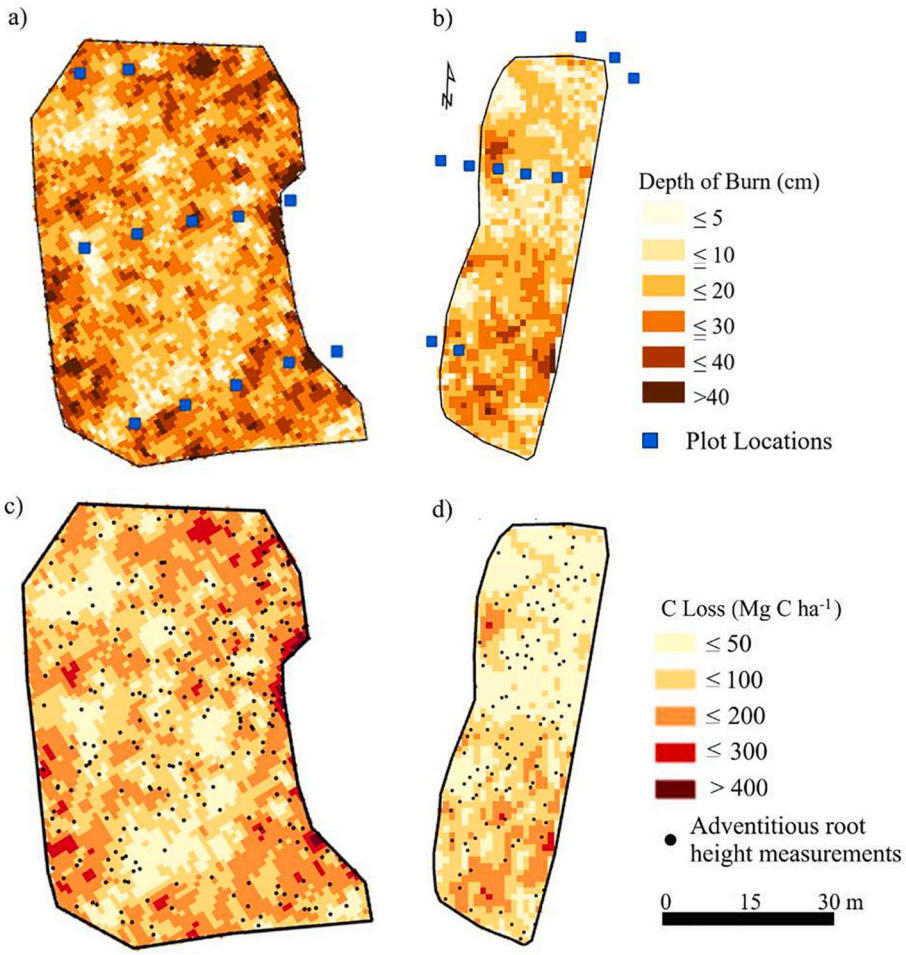


**Fig. 4.** Depth of burn interpolated from adventitious roots per geographically located tree in a) moist and drier sites. Consumption of the duff layer is used to calculate C loss from unburned duff layer cores (7) and (8) for the same sites: c) moist and d) dry.

**Table 1**
Summary of tree structure measurements per plot (M = moist; D = dry) and C losses determined from allometrically derived biomass for instantaneous (combusted) and longer term (eventual decomposition) tree components within south, centre and north plots. F/S represents the ratio of fallen trees to standing dead trees three years after the fire.

| Plot | Average dbh (cm) (st. dev.) | Average Height (m) (st. dev) | Standing Stems/ ha | F/S Ratio | Instantaneous Tree C Loss (Mg C ha$^{-1}$) (st. dev) | Long Term Tree C Loss (Mg C ha$^{-1}$) (st. dev) | Total Tree C Loss (Mg C ha$^{-1}$) (st. dev) |
|---|---|---|---|---|---|---|---|
| MSouth | 26.7 (15.1) | 17.58 (9.08) | 600.00 | 0.11 | 16.47 (17.49) | 96.56 (79.32) | 113.03 (4.24) |
| MCenter | 24.9 (9.9) | 15.85 (8.16) | 1000.00 | 0.20 | 17.55 (8.31) | 109.06 (38.80) | 126.61 (2.04) |
| MNorth | 22.5 (14.3) | 13.76 (8.25) | 675.00 | 0.26 | 17.85 (10.36) | 84.57 (58.57) | 102.46 (3.34) |
| DSouth | 20.9 (5.0) | 19.22 (2.67) | 975.00 | 0.24 | 13.85 (3.39) | 90.86 (17.67) | 104.71 (1.03) |
| DCenter | 20.4 (5.0) | 18.03 (3.33) | 900.00 | 0.22 | 11.74 (3.61) | 72.50 (15.90) | 84.23 (0.91) |
| DNorth | 18.2 (5.6) | 15.60 (3.96) | 1075.00 | 0.14 | 9.72 (3.13) | 62.17 (19.22) | 71.89 (1.10) |
| M Average | 24.7 (1.7) | 15.73 (8.50) | 758 | 0.19 | 17.29 (12.05) | 96.73 (58.89) | 114.03 (3.20) |
| D Average | 19.9 (5.2) | 17.62 (3.32) | 983 | 0.20 | 11.77 (3.37) | 75.18 (17.59) | 86.94 (1.01) |

### 3.3. Loss of C from soils vs. Trees and short vs. long-term losses

Patterns of C loss from fire at the riparian site observed in soil and tree biomass were magnified when we examined the total C loss from both sites. In the moist riparian site, total C loss from combined soil and tree biomass is an average of 206.93 Mg C ha$^{-1}$. Comparatively, total C loss from the drier upland site is 144.94 Mg C ha$^{-1}$ (Fig. 6). Near half (45%) of total C loss at the riparian site was associated with soil C loss, indicating the magnitude of deep peat combustion in productive sub-alpine and montane forests.

Soil C loss also represents C consumption during fire where a pulse of C was removed from the ecosystem with the flaming front and immediately after the fire in smoldering combustion. In riparian mountain valleys containing deep soil peat layers, 53% of the C loss from soils and trees occurs during the initial combustion phase, while the remaining 47% is released over decades when dead standing trees eventually fall and remaining stem/branch biomass breaks down and decomposes (Fig. 6). In drier valley forests, there is a shift in the proportion of total C release to long-term losses associated with tree stem/branch decomposition (52%; Fig. 6), however, it is likely that these slight differences are within the range of error. Overall, initial soil and tree C losses associated with combustion represent about half of the total C lost, with greater overall loss of C from the moist, (more) productive pre-fire riparian forest (Figs. 5, 6).

### 3.4. Scaling C loss using multi-spectral lidar-based intensity metrics: aNBR

Here, we have demonstrated the proportional contributions of soil and tree biomass C losses during the period of initial combustion and over decades as trees eventually fall and decompose. Quantifying these losses over broad areas is logistically challenging due to field measurement constraints and limitations of optical remotely sensed data. Lidar remote sensing captures measurements of ground surface elevation and vegetation structures. When lidar surveys were collected pre- and post-fire, elevation differences can be determined associated with depth of burn (e.g. Alonzo et al., 2017; Chasmer et al. 2017; McCarley et al. 2020). Multi-spectral lidar data offer the potential to differentiate between post-fire standing tree structures and variations in scorching of the ground surface, among other vegetation structural and reflection-based metrics (e.g. Hopkinson et al. 2016; Chasmer et al. 2017), which may be related to losses of C.

Despite greater losses of biomass at the moist riparian site, using the ratio of NIR and SWIR laser return intensity wavelengths determined within one year post-fire, we find greater negative aNBR within the dry valley site (avg = -0.46; st. dev. ± 0.16), whereas the moist site exhibits a less negative aNBR (avg = −0.25; st. dev. ± 0.08). This difference in aNBR between the two sites (*t*-test: $p < 0.001$) is consistent with field observations of early commencement of patchy herb regeneration in the moist site, while little to no vegetation regeneration was observed in the drier site in summer 2018. Higher soil moisture found at the riparian site also increased SWIR absorption, resulting in a reduction in the apparent severity (represented by less negative aNBR found near the stream (Fig. 7)). Fig. 7 illustrates spatial variability of NIR and SWIR gridded ground-surface intensity data as well as aNBR. Patches of regenerating vegetation were observed in reduced aNBR and higher NIR intensity reflections within the moist site while greater absorption of NIR and reflection of SWIR was observed in the drier upland site. These factors, which may be difficult to isolate in a band ratio such as aNBR, complicate the relationship between loss of soil C associated with depth of burn and aNBR. This is also a limitation or uncertainty of optical remote sensing fire indices used to estimate burn severity in areas of open canopy or limited canopy cover (e.g. in open peatlands).

We found no relationship between measured or interpolated depth of burn in either the moist riparian site ($R^2 = 0.002$; 0.0009, n = 299 trees) or the drier site ($R^2 = 0.05$; 0.05, n = 137 trees) with lidar-intensity-

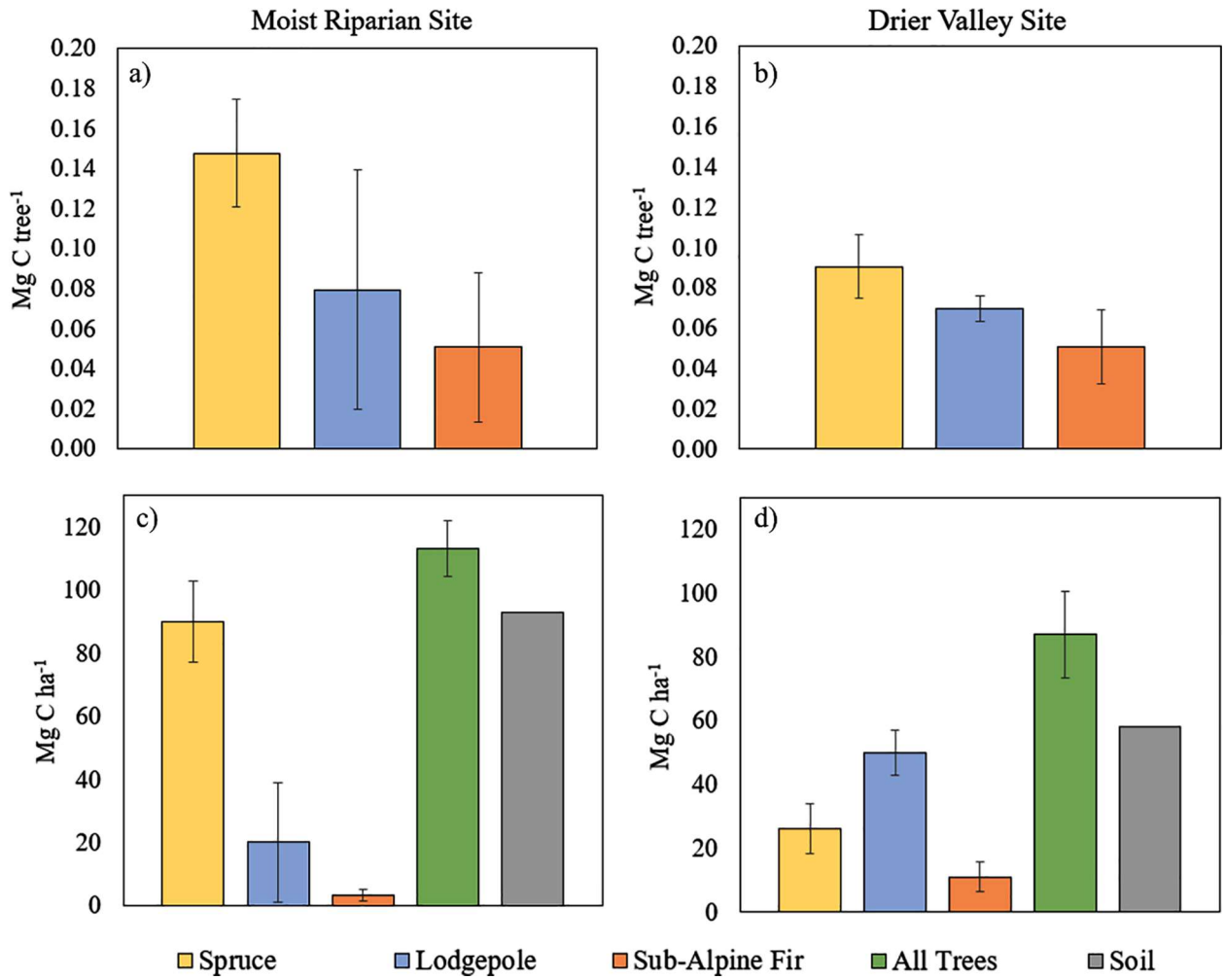


**Fig. 5.** Comparison of carbon losses per tree species on a per tree basis at a) moist and b) drier valley sites, and a per area basis at c) moist and d) drier sites. Soil C losses are added for comparison in (c) and (d). Values are means of plot totals ± std.dev.

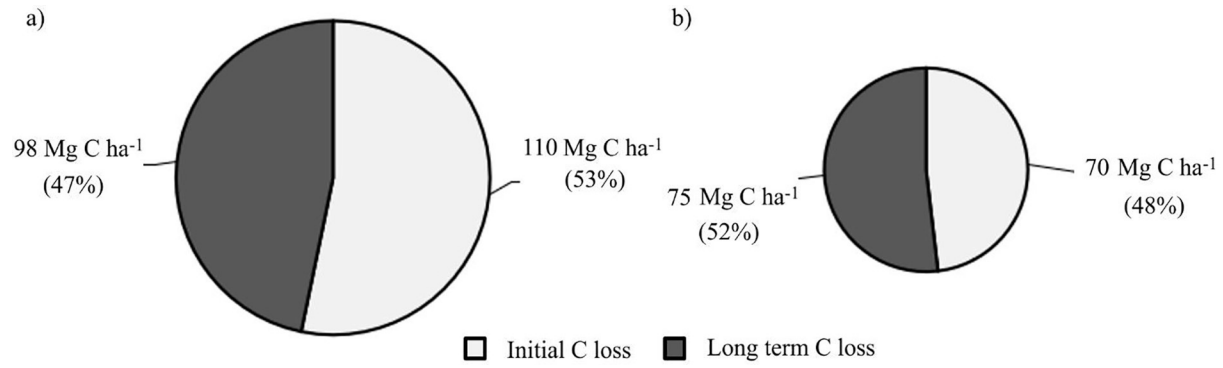


**Fig. 6.** Circle plots of long-term vs initial C losses in a) moist riparian vs. b) drier valley sites. The diameter size of the circles illustrates the proportional total carbon loss.

derived aNBR, though the relationship was improved at the drier site. This illustrates the complexity associated with determining loss of ground surface organic soils compared with intensity-based metrics from SWIR and NIR, which are similarly used in optical remote sensing. The interaction between laser intensity and ground surface characteristics at the time of survey have a greater influence on reflected energy in NIR and SWIR as this relates to the aNBR.

Fig. 8 illustrates the relationship between proportion of vegetation, charred soil surface and charred + mineral soil surface (total soil proportion) within 1 $m^2$ plots at the two sites. Here we found expected relationships between aNBR and proportion of vegetation and soil surfaces in the drier site, such that greater amounts of post-fire vegetation growth in the year following the fire corresponded with reduced negative values of aNBR ($R^2 = 0.32$, $p = 0.003$) (Fig. 8a). The proportion of burned soil within plots was also related to aNBR as was the proportion of charred soils, as they were differentiated from more reflective mineral

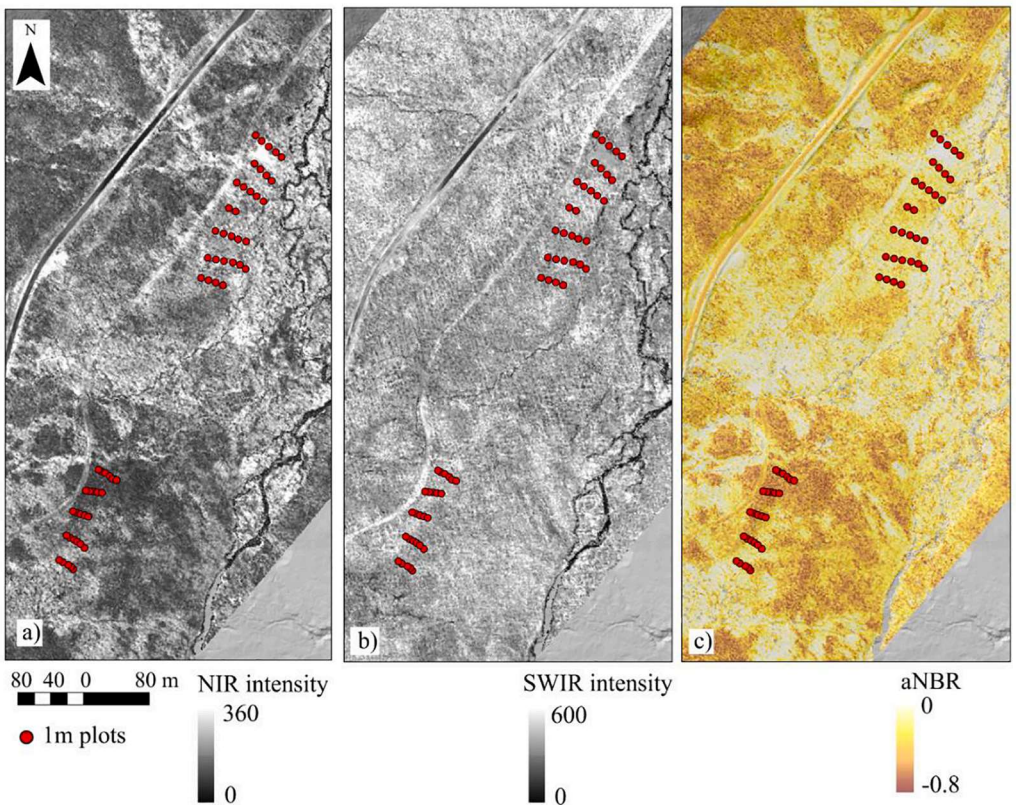


**Fig. 7.** Gridded lidar return intensity data in a) NIR and b) SWIR wavelengths; c) aNBR, where increasingly negative burn index indicates greater burn severity. 1 m × 1 m plots are illustrated for the moist riparian site (northern plots) and the drier site (southern plots) used to determine proportion of charred and mineral soils, and early vegetation regeneration.

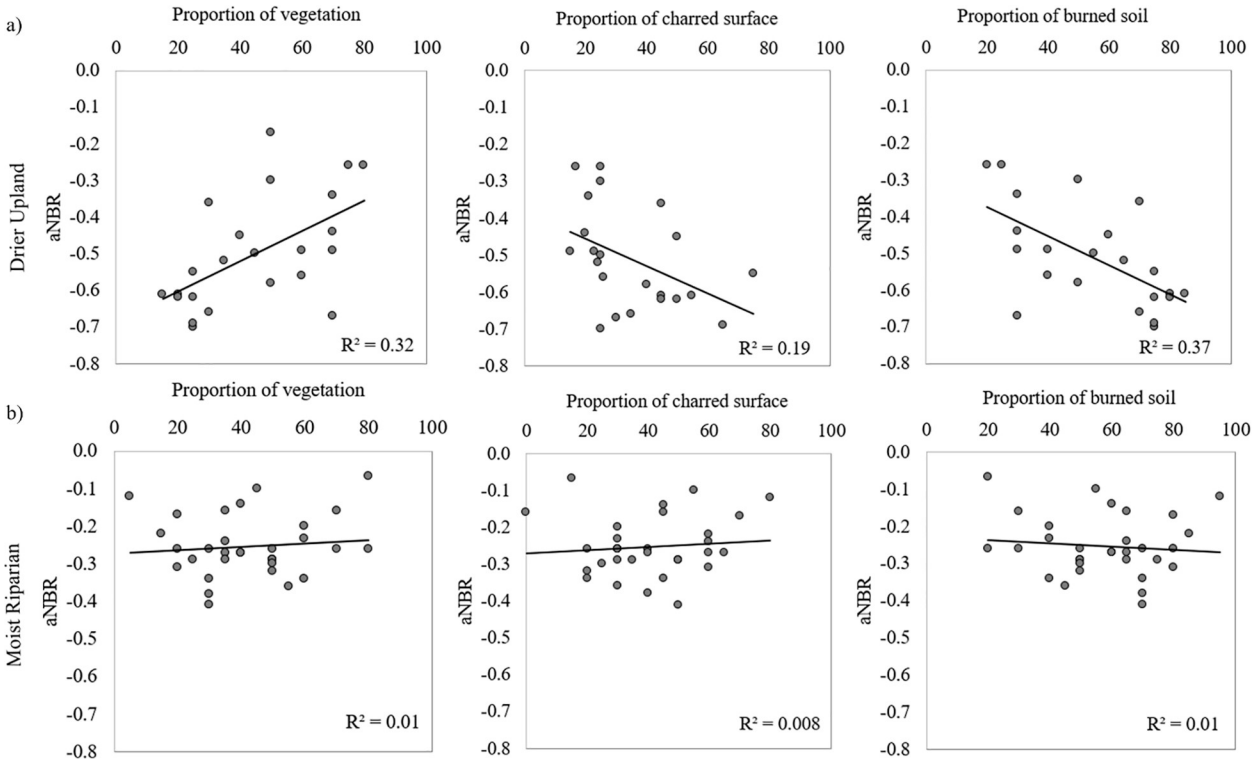


**Fig. 8.** Linear regressions between aNBR, vegetation, charred surfaces, and total burned soil (char + mineral soil) proportions at a) the drier upland site; b) moist riparian site.

soils ($R^2 = 0.19$, $p = 0.04$) and total soil proportion ($R^2 = 0.37$, $p = 0.003$). We did not find strong relationships between aNBR and surface characteristics in plots in the riparian site (Fig. 8b). This may have been due to the combination of different vegetation species, more rapid growth, and the higher moisture content of soils, illustrating a further need to explore the interactions between laser intensity reflections used for calculation of aNBR. Further, we report that slope and elevation did not have an influence on laser return intensity at these sites ($R^2 < 0.01$, not shown).

## 4. Discussion

In this study we find that a lower riparian landscape position in montane forests with moist soils contain greater amounts of C stored in tree and soil biomass compared with nearby upper landscape position sites that are characterised by drier soil conditions. Though soil C is a significant component of montane valley bottom ecosystems, C storage may be reduced with elevation, where soils are generally drier—thereby reducing the total overall C of this mountain valley ecosystem. Even so, C stocks presented here indicate that overstory C in WLNP (87–114 Mg C $ha^{-1}$) appears to be at the low end of stand level C density in montane cordilleran forests as Stinson et al. (2011) suggest that C stocks are ~275 Mg C $ha^{-1}$ for the western interior Cordilleran ecozone of Canada. However, this comparison requires a broader study on C stocks in WLNP. It is also notable that we could not estimate pre-fire aboveground biomass from understory shrubs or detritus, which is normally included in the total aboveground biomass compartment as described in Stinson et al., (2011) or Law et al. (2003). Shrubs consisted of 5–10% forest plot coverage when measured in 2000 (Parks Canada unpublished data), but were not observed at these two sites prior to the Kenow fire. If we compare our findings from productive montane valleys in the southern Cordillera region to C quantification studies in nearby regions, we find that C stocks were also generally higher in similar forests in central British Columbia (BC) (Freeden et al., 2005) and northern interior forests of the USA (Bisbing et al., 2010), though are lower compared with sites in central BC. Carbon dense high biomass regions were also noted in the Pacific Norwest and south-central boreal regions (Law et al., 2003; Goulden et al., 2011). Freeden et al., (2005) found that total C stocks for similar old growth stands with white spruce and Engelmann spruce were between 119 and 155 Mg C $ha^{-1}$ for trees (excluding roots) in central BC. Comparisons to montane forests of the interior USA appear similar as Bisbing et al., (2010) quantify C stocks in Northwestern Montana and find that overstory trees store between 134 and 156 Mg C $ha^{-1}$, and Chatterjee et al., (2009) determine that aboveground biomass in unmanaged lodgepole pine forests in Wyoming store 172 Mg C $ha^{-1}$. Law et al., (2003) found that live aboveground biomass in old growth ponderosa pine forests of central Oregon range from 122 to 157 Mg C $ha^{-1}$ exceeding quantities of overstory C in WLNP by an additional 40%.

Soil C stocks in central BC forests decline with depth, and range from 106 to 115 Mg C $ha^{-1}$ (Freeden et al., 2005), whereas we find that soil C increases with depth down to the mineral substrate due to the density of peat and moss groundcover. Here, soil C loss ranges from 58 to 93 Mg C $ha^{-1}$. Comparisons to montane forests of the interior USA are similar to WLNP, as Bisbing et al. (2010) found that mineral soils store 50–82 Mg C $ha^{-1}$, and Chatterjee et al., (2009) found 77.5 Mg C $ha^{-1}$ in belowground sources. Law et al., (2003) found that soil C ranges from 56 to 65 Mg C $ha^{-1}$, which is 69% – 96% of the soil C losses we found in the southern Canadian Rockies.

The comparison of C compartments between other montane valley sites and WLNP is also somewhat limited as the location of the park, at the southeast corner of the Canadian Montane Cordilleran ecozone, is relatively understudied in terms of soil C accumulation, fire history, and stand dynamics (Marcoux et al., 2015). We observed 100% canopy mortality in WLNP, so direct comparisons between overstory C loss here, and C stocks of unburned canopies in forests can be inferred from other regions (e.g. Law et al., 2003; Bisbing et al., 2010). However, our soil C loss quantities cannot be compared directly to quantifications of total ecosystem soil C as combustion losses do not represent the total C stock. Even so, soil C loss quantities were comparable to total ecosystem soil C levels in interior regions of the northwestern USA and interior BC (Bisbing et al., 2010; Law et al., 2003; Freeden et al., 2005; Chatterjee et al, 2009). This indicates that either a large percentage of total soil C in our sites was combusted in the Kenow fire, or moist conditions near the continental divide make this region particularly C dense. As soil C is combusted during and immediately following the fire due to transfer of energy from the canopy into organic soils (Thompson et al., 2015), soil C combustion contributes to large increases in emissions from wildfire. Meigs et al., (2009) estimate that C emissions for fires in northwestern US range from 17 to 32 Mg C $ha^{-1}$. The inclusion of soil C combustion into these estimations substantially increases the quantity of direct C emissions from fires illustrated in Fig. 5. Including soils, the dry site lost 70 Mg C $ha^{-1}$, a number 2–3 times larger than standard estimations (Meigs et al., 2009), with potential to be even greater in productive riparian and transitional areas (Fig. 6). For perspective, an average passenger vehicle emits 1.75 Mg C annually (Environmental Protection Agency, 2018), making the per ha soil C losses calculated here equivalent to the annual carbon emissions of 53 typical passenger vehicles (moist site) versus 33 vehicles (dry site).

Recent increases in North American fire activity suggests that climatic warming and drying along with a shift in the timing of hydrological regimes (Littell et al., 2009; Westerling, 2016) increases the availability of combustible fuel (Flannigan et al., 2016). The impacts of these changes have increased fire frequency and reduced return intervals, increased fire severity, and expanded fire extent (Kasischke and Turetsky, 2006; Steel et al., 2015; Reilly et al., 2017). Fire season warming and drying effects are predicted to continue to increase in the future, along with associated changes in fire behaviour across North America (Wang et al., 2017; Flannigan et al., 2016; Wotton et al., 2017). Montane Cordilleran forests and those of the central Rockies and Pacific Northwest may be particularly susceptible to changes in climate and fire activity as mountainous regions have historically been snow free for only 2–4 months, thus limiting potential fire activity (Westerling, 2016). Now, climatic conditions and wildland fire regimes in mountainous regions are significantly different from the last time forests re-established following a fire disturbance (Westerling, 2016), which may have implications on the way these ecosystems respond.

If forested mountain ecosystems are to become drier and burn more frequently as the literature suggests, we draw attention to our findings that between 86 and 88% of tree biomass remained for long term decomposition and was not significantly different between moist riparian vs. dry upland valley sites (Table 1). However, soil C losses are significantly different between sites (58 Mg C $ha^{-1}$ at the drier valley site vs 92 Mg C $ha^{-1}$ at the moist riparian site; Table 1, Fig. 5). This indicates that initial pulses of C from fires in these regions were heavily influenced by organic soil combustion and are spatially variable. Given the exposure of mineral soils and depletion of organic soils at the dry site, areas of local topographic depressions could become important post-fire C stores, while the ability to sequester C into biomass may decline as local topographical gradients increase moisture limitations. However, if the Kenow fire is an indication of future extreme fire years in a changing climate, the C storage capacity of wet riparian sites in valley bottoms could also be vulnerable to large C losses from combustion (Figs. 5 and 6).

Despite these results and the need to understand the contribution of soil C to wildland fire C dynamics (Fellows et al., 2018; Wilkinson et al., 2018; Boby et al., 2010), the major limitation has been the difficulty associated with quantifying pre-fire soil and understory C variations over large and often remote areas. The normalised burn ratio (NBR) derived from optical remotely sensed data has been used extensively to better understand fire extent and severity in expansive, remote areas by taking advantage of post-fire reflectance characteristics of the shortwave infrared part of the electromagnetic spectrum. This has been used to

estimate biomass combustion by comparing the difference between pre- and post-fire reflectance/absorptance characteristics of the land surface (the differenced normalised burn ratio, dNBR, and others, García and Caselles, 1991). Despite wide use, optical image characterisation of burn severity using the NBR and the less sensitive normalised difference vegetation index (NDVI) (Chen et al., 2020) can be prone to individual uncertainties of up to ~6% mostly associated with timing of image pair collection and seasonality illustrated in Chen et al. (2020), as well as a combination of environmental conditions (Boucher et al. 2017), shadowing (Hoy et al. 2008; Verbyla et al. 2008), and topographic variability (Verbyla et al. 2008).

In addition to these uncertainties, one of the major limitations of the use of dNBR and other optical remote sensing-based indices for quantifying total ecosystem C loss is due to occlusion of pre-fire soil and understory by the tree canopy envelope. Here, we find that between 35% (dry) to 45% (moist) of total C loss during combustion is due to deep burning of the soil organic matter and mosses (Fig. 5). These results indicate that the proportion of organic soil/understory C represents a substantial part of the overall C that may be consumed. Excluding below canopy losses due to occlusion may result in significant underestimation of C loss using optical remotely sensed data. Results from Hoy et al. (2008) agree with this observation as they found low correlation between the consumption of the organic soil layer determined from field-based composite burn index (CBI) and Landsat ETM + burn severity indices in burned boreal black spruce stands, resulting in ~30% underestimate of C loss compared with field measurements. Hoy et al. (2008) conclude that optically-based fire indices may be more appropriate for low to moderate severity crown fire. Boucher et al. (2017), on the other hand, found strong correspondence between dNBR and CBI in eastern Canadian boreal black spruce and jack pine forests, however they note that, pre-fire conditions and burn severity is highly variable between sites. Similar results were also found in Whitman et al. (2018) who compared three remotely sensed indices with field-based burn severity indices. They found that overstory plot indices corresponded best with remotely sensed severity indices, but corresponded less with the Burn Severity Index, which incorporates estimates of charred soil surface. Uncertainties associated with burn severity indices could have considerable implications especially for C-climate-feedback modelling/understanding in northern and montane ecosystems where cool/cold and moist conditions inhibit organic soil decomposition and climate-mediated atmospheric drying enhance soil fuel availability (Turetsky et al. 2015).

To address this gap in understanding, lidar provides a continuous "plot-based" method from which uncertainties from optical remote sensing can be identified across a broad range of environmental characteristics (e.g. McCarley et al. 2020). In this study, short- and long-term C losses were determined using a combined field-lidar approach at two endmember valley sites. Pre- and post-fire lidar data offer the potential to determine canopy, understory, and soil biomass losses, providing an opportunity to quantify some of the uncertainties associated with optical indices (Chasmer et al. 2017). While optical remote sensing indices were not compared with lidar data in this study, we found that multi-spectral lidar data may have utility to improve quantification of post-fire soil characteristics because this provides both canopy structural as well as surface spectral information. The utility of multi-spectral airborne lidar is becoming apparent for pre-fire species identification (Hopkinson et al. 2016; Budei et al. 2018), spectral vegetation indices (Okhrimenko et al. 2019), and successful identification and modelling of coarse woody debris beneath forested canopies (Queiroz et al. 2020). The use of multi-spectral lidar bypasses a persistent problem in the effective optical remote sensing of surface level burn/fire severity: the interaction of incoming and outgoing energy with burned or partially burned canopies and understory vegetation (Gibson et al., 2020; Chasmer et al., 2017).

Understory and ground surface species classification are a tangible 'next step' for the use of multi-spectral lidar for fire fuel modelling and post-fire ecosystem recovery. Here, successful differentiation between charred/mineral soils and vegetation was observed, however this was not without the potentially confounding influence of surface soil moisture on laser absorption at 1550 nm at the riparian site. Interaction with remaining tree biomass can also influence laser pulses, however, this can be avoided by using single return laser intensity from ground at 1064 nm and 1550 nm to reduce pulse attenuation from split and secondary returns that have intercepted remaining biomass (e.g., Hopkinson & Chasmer, 2009). Uncertainties remain in the correlation between multi-spectral lidar derived aNBR and depth of burn, which is closely related to C loss. These occur because higher reflectance of charred soils in near and shortwave infrared wavelengths (1064 nm and 1550 nm) do not correlate well with depth of burn (Figs. 7 and 8), which is also a limitation of optical imagery. Despite this, one could hypothesize that a decrease of depth to water table/surface water interactions with 1550 nm could be correlated with deep burns in some areas, while machine learning may be used to characterise environmental/lidar-based thematic influences on depth of burn. In this study, we found stronger correlations between single wavelength intensity returns and proportions of charred and mineral soils. These results could provide useful information of post-fire soil condition and suitability for rapid vegetation regeneration. Goetz et al. (2012) note the importance of recalcitrant char as it contributes to post-fire soil productivity and C storage, yet linkages between char and other environmental drivers remain poorly understood. The ability of multi-spectral lidar to identify char vs mineral soil and vegetation in grid cell intensity mixtures at fine spatial scales could be an important area of future ecological/regeneration research combined with lidar thematic data within a deep learning/artificial intelligence framework to be developed.

### 4.1. Limitations

To quantify soil carbon losses, we measured adventitious root height in the summers of 2019 (moist site) and 2020 (drier site), two and three years following the Kenow fire respectively. Wildfires remove protective vegetation and litter, alter soil structures and can enhance water repellency of soils. These factors result in more rainfall striking the soil directly and can cause enhanced erosion and thinning of soils on hillslopes (Moody et al., 2013; Shakesby & Doerr, 2006). Shakesby & Doerr (2006) find that these effects can result in large but highly variable soil surface loss rates of between 0.1 and 41 Mg soil ha $^{-1}$ per year depending on the severity of the fire and local conditions. Notably, these heightened erosion rates are usually limited to the first months after the fire and are usually reduced at larger spatial scales due to redeposition of soil (González-Pérez et al., 2004).

As we were not able to measure the erosion rates of soils and measured adventitious root height 2–3 years following the fire, there may be some areas of overestimation (from erosion) and some underestimation (areas of deposition) of soil C loss to combustion in some locations. A seasonal stream near the wet riparian site is prone flooding in spring, thereby removing additional soil from tree roots. To mitigate this influence, we excluded soil C loss measurements within 10 m of the stream. Uncertainties also exist in meltwater rills and areas of localized erosion. However, we observed only 14 of 313 trees (4.4%) at the moist site that displayed noticeable evidence of rill erosion. Further, both sites, especially the moist riparian site, are not greatly topographically variable, thereby minimizing the effect of soil erosion and deposition at the site level. Future research will quantify rates of post-fire areas of erosion and deposition using multi-temporal lidar data.

### 4.2. Conclusions

In this study, we examined the proportion of C lost from trees and soils due to combustion from a moist riparian and drier valley site in a productive montane valley in Southern Alberta, Canada. Secondly, we compared post-fire soil characteristics to vegetation indices derived from airborne multispectral lidar data to provide a framework for

scaling the spatial variability of C losses from trees and soils. We find that C losses are slightly greater from tree components than soil components and that C loss is greater in moist riparian areas than drier valley areas. Soil C loss plays a substantial role in driving large, instantaneous C losses from both sites, with a greater influence in the moist riparian site.

Signal intensity data from multispectral lidar is influenced by the proportion of post-fire regeneration, soils depleted of organic matter (mineral soils) and those with remaining organic matter (charred soils) and may have utility for quantifying post-fire soil variability for evaluating post-fire burn indices from optical remotely sensed data. As montane forests in the southern Canadian Cordilleran zone change in the future due to warming and drying, we may expect to see a decrease in productivity and increased fire return intervals. This could significantly reduce the C sequestration potential of these forests while also reducing overall stand age. Changes in fire return interval in addition to more severe fires could increase the probability of these forests becoming an overall net source of C over the lifespan of these forests (from regeneration to combustion). Understanding the net balance between the rates of C uptake from rapidly regenerating vegetation following fire and rates of combustion-driven C losses, such as described here, is crucial to understanding how forests in this region respond to and are influenced by climate-fire interactions in the future.

## CRediT authorship contribution statement

**S. Gerrand:** Conceptualization, Methodology, Validation, Formal analysis, Investigation, Writing - original draft, Writing - review & editing, Visualization. **J. Aspinall:** Methodology, Validation, Formal analysis. **T. Jensen:** Methodology, Validation, Formal analysis. **C. Hopkinson:** Methodology, Resources, Data curation, Funding acquisition. **A. Collingwood:** Validation, Resources, Funding acquisition. **L. Chasmer:** Conceptualization, Methodology, Formal analysis, Resources, Writing - review & editing, Visualization, Supervision, Project administration, Funding acquisition.

## Declaration of Competing Interest

The authors declare that they have no known competing financial interests or personal relationships that could have appeared to influence the work reported in this paper.

## Acknowledgements

The authors would like to acknowledge the support for research provided by Parks Canada (grant number GC-1158), NSERC Discovery Grant funding to Chasmer (grant number 2017-04492) and Hopkinson (grant number 2017-04362) and a University of Lethbridge Start-up Grant to Chasmer. The Teledyne Optech Inc. Titan lidar system has been provided via a grant to Hopkinson by Western Economic Diversification Canada (grant number 000015316), GNSS and other equipment was funded by Canadian Foundation for Innovation (grant number 32436). Hopkinson acknowledges Alberta Environment and Parks for eastern slopes water and vegetation research, which supported field assistance (grant number 19GRAEM26). Gerrand acknowledges funding provided by the NSERC Undergraduate Student Research Award for the summer of 2020, with additional stipend from Canada Wildfire NSERC-SPG-N. Aspinall acknowledges funding and scholarship support from the University of Lethbridge. In addition to funding, Gerrand acknowledges the field assistance from several undergraduate and graduate students: Jacob Martin, Emily Jones, Edberto Moura-Lima, Chinyere Ottah, Humaira Enayetullah, Nick Cuthbertson, Celeste Barns and Rachelle Shearing. Emily Jones is thanked for her assistance with soil sample processing. Finally, we would like to thank Down To Earth Labs of Lethbridge Alberta for providing additional laboratory resources and support for soil bulk density and C analysis.

## References

Alonzo, M., Morton, D.C., Cook, B.D., Andersen, H.-E., Babcock, C., Pattison, R., 2017. Patterns of canopy and surface layer consumption in a boreal forest fire from repeat airborne lidar. Environ. Res. Lett. 12.

Bartowitz, K.J., Higuera, P.E., Shuman, B.N., Mclauchlan, K.K., Hudiburg, T.W., 2019. Post-fire carbon dynamics in subalpine forests of the rocky mountains. Fire 2 (4), 58. https://doi.org/10.3390/fire2040058.

Bisbing, S., Alaback, P., Deluca, T., 2010. Carbon storage in old-growth and second growth fire dependent western larch (Larix occidentalis Nutt.) forests of the Inland Northwest, USA. For. Ecol. Manage. 259 (5), 1041–1049. https://doi.org/10.1016/j.foreco.2009.12.018.

Boby, L.A., Schuur, E.A.G., Mack, M.C., Verbyla, D., Johnstone, J.F., 2010. Quantifying fire severity, carbon, and nitrogen emissions in Alaskas boreal forest. Ecol. Appl. 20 (6), 1633–1647. https://doi.org/10.1890/08-2295.1.

Boucher, J., Beaudoin, A., Hébert, C., Guindon, L., Bauce, É., 2017. Assessing the potential of the differenced Normalized Burn Ratio (dNBR) for estimating burn severity in eastern Canadian boreal forests. Int. J. Wildland Fire 26 (1), 32–45.

Budei, B.C., St-Onge, B., Hopkinson, C., Audet, F.A., 2018. Identifying the genus or species of individual trees using a three-wavelength airborne lidar system. Remote Sens. Environ. 204, 632–647.

Carter, M.R., Gregorich, E.G., 2010. Soil Sampling and Methods of Analysis. Taylor & Francis/CRC Press, S.l.

Chasmer, L.E., Hopkinson, C.D., Petrone, R.M., Sitar, M., 2017. Using multitemporal and multispectral airborne lidar to assess depth of peat loss and correspondence with a new active normalized burn ratio for wildfires. Geophys. Res. Lett. 44 (23) https://doi.org/10.1002/2017gl075488.

Chatterjee, A., Vance, G.F., Tinker, D.B., 2009. Carbon pools of managed and unmanaged stands of ponderosa and lodgepole pine forests in Wyoming. Can. J. For. Res. 39 (10).

Coen, G.M., Holland, W.D., 1976. Soils of Waterton Lakes National Park, Alberta.

Chen, D., Loboda, T.V., Hall, J.V., 2020. A systematic evaluation of influence of image selection process on remote sensing-based burn severity indices in North American boreal forest and tundra ecosystems. ISPRS J. Photogramm. Remote Sens. 59, 63–77.

Eisenberg, C., Anderson, C.L., Collingwood, A., Sissons, R., Dunn, C.J., Meigs, G.W., Edson, C.B., 2019. Out of the ashes: ecological resilience to extreme wildfire, prescribed burns, and indigenous burning in ecosystems. Front. Ecol. Evolut. 7 https://doi.org/10.3389/fevo.2019.00436.

Environmental Protection Agency, 2018. Greenhouse Gases Equivalencies Calculator: Calculations and References. Retrieved December 04, 2020, from https://www.epa.gov/energy/greenhouse-gases-equivalencies-calculator-calculations-andreferences.

Fellows, A.W., Flerchinger, G.N., Lohse, K.A., Seyfried, M.S., 2018. Rapid recovery of gross production and respiration in a mesic mountain big sagebrush ecosystem following prescribed fire. Ecosystems 21 (7), 1283–1294. https://doi.org/10.1007/s10021-017-0218-9.

Flannigan, M.D., Wotton, B.M., Marshall, G.A., Groot, W.J.D., Johnston, J., Jurko, N., Cantin, A.S., 2016. Fuel moisture sensitivity to temperature and precipitation: climate change implications. Clim. Change 134 (1–2), 59–71. https://doi.org/10.1007/s10584-015-1521-0.

Fraser, R.H., Van der Sluijs, J., Hall, R.J., 2017. Calibrating satellite-based indices of burn severity from UAV-derived metrics of a burned boreal forest in NWT, Canada. Remote Sensing. 9 (3), 279.

Freeden, A.L., Bois, C.H., Janzen, D.T., Sanborn, P.T., 2005. Comparison of coniferous forest carbon stocks between old-growth and young second-growth forests on two soil types in central British Columbia, Canada. Canadian J. Forest Res. 35 (6), 1411–1421.

Friedlingstein, P., Jones, M.W., O'sullivan, M., Andrew, R.M., Hauck, J., Peters, G.P., Peters, W., Pongratz, J., Sitch, S., Quéré, C.L., Bakker, D.C., et al., 2019. Global carbon budget 2019. Earth Syst. Sci. Data 11 (4), 1783–1838.

García, M.L., Caselles, V., 1991. Mapping burns and natural reforestation using Thematic Mapper data. Geocarto Int. 6 (1), 31–37.

Gibson, R., Danaher, T., Hehir, W., Collins, L., 2020. A remote sensing approach to mapping fire severity in south-eastern Australia using sentinel 2 and random forest. Remote Sens. Environ. 240, 111702 https://doi.org/10.1016/j.rse.2020.111702.

Goetz, S.J., Bond-Lamberty, B., Law, B.E., Hicke, J.A., Huang, C., Houghton, R.A., McNulty, S., O'Halloran, T., Harmon, M., Meddens, A.J.H., Pfeifer, E.M., Mildrexler, D., Kasischke, E.S., 2012. Observations and assessment of forest carbon dynamics following disturbance in North America. J. Geophys. Res. Biogeosci. 117, 0148–0227.

Gongalsky, K.B., Persson, T., 2013. Recovery of soil macrofauna after wildfires in boreal forests. Soil Biol. Biochem. 57, 182–191. https://doi.org/10.1016/j.soilbio.2012.07.005.

González-Pérez, J.A., González-Vila, F.J., Almendros, G., Knicker, H., 2004. The effect of fire on soil organic matter—a review. Environ. Int. 30, 855–870.

Goulden, M.L., McMillan, A.M.S., Winston, G.C., Rocha, A.V., Manies, K.L., Harder, J.W., Bond Lamberty, B.P., 2011. Patterns of NPP, GPP, respiration, and NEP during boreal forest succession. Global Change Biol. 17, 855–871.

Greene, D.F., Macdonald, S.E., Haeussler, S., Domenicano, S., Noël, J., Jayen, K., Swift, L., 2007. The reduction of organic-layer depth by wildfire in the North American boreal forest and its effect on tree recruitment by seed. Can. J. For. Res. 37 (6), 1012–1023. https://doi.org/10.1139/x06-245.

Harden, J.W., O'Neill, K.P., Trumbore, S.E., Veldhuis, H., Stocks, B.J., 1997. Moss and soil contributions to the annual net carbon flux of a maturing boreal forest. J. Geophys. Res. 102 (D24), 28805–28816. https://doi.org/10.1029/97JD02237.

Hall, R.J., Freeburn, J.T., De Groot, W.J., Pritchard, J.M., Lynham, T.J., Landry, R., 2008. Remote sensing of burn severity: experience from western Canada boreal fires. Int. J. Wildland Fire 17 (4), 476–489.
Hopkinson, C., Chasmer, L., 2009. Testing LiDAR models of fractional cover across multiple forest ecozones. Remote Sens. Environ. 113 (1), 275–288. https://doi.org/10.1016/j.rse.2008.09.012.
Hopkinson, C., Chasmer, L., Gynan, C., Mahoney, C., Sitar, M., 2016. Multisensor and multispectral LiDAR characterization and classification of a forest environment. Canadian J. Remote Sens. 42 (5), 501–520. https://doi.org/10.1080/07038992.2016.1196584.
Hoy, E.E., French, N.H., Turetsky, M.R., Trigg, S.N., Kasischke, E.S., 2008. Evaluating the potential of Landsat TM/ETM+ imagery for assessing fire severity in Alaskan black spruce forests. Int. J. Wildland Fire 17 (4), 500–514.
Huber, U.M., Bugmann, H.K.M., Reasoner, M.A., 2006. Global Change and Mountain Regions: an Overview of Current Knowledge. Springer, Heidelberg.
Hudak, A.T., Kato, A., Bright, B.C., Loudermilk, E.L., Hawley, C., Restaino, J.C., Weise, D. R., 2020. Towards spatially explicit quantification of pre- and postfire fuels and fuel consumption from traditional and point cloud measurements. For. Sci. https://doi.org/10.1093/forsci/fxz085.
Hudiburg, T., Law, B., Turner, D.P., Campbell, J., Donato, D., Duane, M., 2009. Carbon dynamics of Oregon and Northern California forests and potential land-based carbon storage. Ecol. Appl. 19 (1), 163–180. https://doi.org/10.1890/07-2006.1.
IPCC, 2019: Climate Change and Land: an IPCC special report on climate change, desertification, land degradation, sustainable land management, food security, and greenhouse gas fluxes in terrestrial ecosystems. P.R. Shukla, J. Skea, E. Calvo Buendia, V. Masson-Delmotte, H.-O. Pörtner, D. C. Roberts, P. Zhai, R. Slade, S. Connors, R. van Diemen, M. Ferrat, E. Haughey, S. Luz, S. Neogi, M. Pathak, J. Petzold, J. Portugal Pereira, P. Vyas, E. Huntley, K. Kissick, M. Belkacemi, J. Malley, (Eds.). In press.
Irvine, J., Law, B.E., Hibbard, K.A., 2007. Postfire carbon pools and fluxes in semiarid ponderosa pine in Central Oregon. Glob. Change Biol. 13 (8), 1748–1760. https://doi.org/10.1111/j.1365 2486.2007.01368.x.
Jenness, J., 2006. Topographic Position Index (tpi_jen.avx) extension for ArcView 3.x, v. 1.3a. Jenness Enterprises. Available at: http://www.jennessent.com/arcview/tpi.htm.
Kasischke, E.S., Turetsky, M.R., 2006. Recent changes in the fire regime across the North American boreal region—Spatial and temporal patterns of burning across Canada and Alaska. Geophys. Res. Lett. 33 (9), L09703. https://doi.org/10.1029/2006GL025677.
Keeley, J.E., 2009. Fire intensity, fire severity and burn severity: a brief review and suggested usage. Int. J. Wildland Fire 18 (1), 116. https://doi.org/10.1071/wf07049.
Lambert, M.C., Ung, C.-H., Raulier, F., 2005. Canadian national tree aboveground biomass equations. Retrieved from Can. J. For. Res. 35 (8), 1996–2018. https://search-proquest-com.ezproxy.uleth.ca/docview/230522147?accountid=12063.
Lamlom, S.H., Savidge, R.A., 2003. A reassessment of carbon content in wood: variation within and between 41 North American species. Biomass Bioenergy 25 (4), 381–388.
Langmann, B., Duncan, B., Textor, C., Trentmann, J., Werf, G.R.V.D., 2009. Vegetation fire emissions and their impact on air pollution and climate. Atmos. Environ. 43 (1), 107 116. https://doi.org/10.1016/j.atmosenv.2008.09.047.
Law, B.E., Sun, O.J., Campbell, J., Tuyl, S.V., Thornton, P.E., 2003. Changes in carbon storage and fluxes in a chronosequence of ponderosa pine. Glob. Change Biol. 9 (4), 510–524. https://doi.org/10.1046/j.1365-2486.2003.00624.x.
Law, B.E., Hudiburg, T.W., Berner, L.T., Kent, J.J., Buotte, P.C., Harmon, M.E., 2018. Land use strategies to mitigate climate change in carbon dense temperate forests. Proc. Natl. Acad. Sci. 115 (14), 3663–3668. https://doi.org/10.1073/pnas.1720064115.
Littell, J.S., Mckenzie, D., Peterson, D.L., Westerling, A.L., 2009. Climate and wildfire area burned in western U.S. ecoprovinces, 1916–2003. Ecol. Appl. 19 (4), 1003–1021. https://doi.org/10.1890/07-1183.1.
Lybrand, R., Gallery, R., Trahan, N., Moore, D., 2018. Disturbance alters the relative importance of topographic and biogeochemical controls on microbial activity in temperate montane forests. Forests 9 (2), 97. https://doi.org/10.3390/f9020097.
Ma, S., Eziz, A., Tian, D., Yan, Z., Cai, Q., Jiang, M., Ji, C., Fang, J., 2020. Size- and age dependent increases in tree stem carbon concentration: implications for forest carbon stock estimations. J. Plant Ecol. 13 (2), 233–240. https://doi.org/10.1093/jpe/rtaa005.
Marcoux, H.M., Daniels, L.D., Gergel, S.E., Silva, E.D., Gedalof, Z.E., Hessburg, P.F., 2015. Differentiating mixed- and high-severity fire regimes in mixed-conifer forests of the Canadian Cordillera. For. Ecol. Manage. 341, 45–58. https://doi.org/10.1016/j.foreco.2014.12.027.
McCarley, T.R., Hudak, A.T., Sparks, A.M., Vaillant, N.M., Meddens, A.J.H., Trader, L., Mauro, F., Kreitler, J., Boschetti, L., 2020. Estimating wildfire fuel consumption with multitemporal airborne laser scanning data and demonstrating linkage with MODIS-derived fire radiative energy. Remote Sens. Environ. 251, 112114.
Meigs, G.W., Donato, D.C., Campbell, J.L., Martin, J.G., Law, B.E., 2009. Forest fire impacts on carbon uptake, storage, and emission: the role of burn severity in the Eastern Cascades, Oregon. Ecosystems 12, 1246–1267.
Meigs, G.W., Krawchuk, M.A., 2018. Composition and structure of forest fire refugia: what are the ecosystem legacies across burned landscapes? Forests 9 (5), 243.
Moody, J.A., Shakesby, R.A., Robichaud, P.R., Cannon, S.H., Martin, D.A., 2013. Current research issues related to post-wildfire runoff and erosion processes. Earth Sci. Rev. 122, 10–37.
Okhrimenko, M., Coburn, C., Hopkinson, C., 2019. Multi-spectral lidar: Radiometric calibration, canopy spectral reflectance, and vegetation vertical SVI profiles. Remote Sensing 11 (13), 1556.
Pacala, S.W., 2001. Consistent land- and atmosphere-based U.S. carbon sink estimates. Science 292 (5525), 2316–2320. https://doi.org/10.1126/science.1057320.
Parks Canada, 2019. Waterton Lakes National Park: Nature and Science. https://www.pc.gc.ca/en/pn-np/ab/waterton/nature.
Perry, D.A., Hessburg, P.F., Skinner, C.N., Spies, T.A., Stephens, S.L., Taylor, A.H., Riegel, G., 2011. The ecology of mixed severity fire regimes in Washington, Oregon, and Northern California. For. Ecol. Manage. 262 (5), 703–717. https://doi.org/10.1016/j.foreco.2011.05.004.
Pribyl, D.W., 2010. A critical review of the conventional SOC to SOM conversion factor. Geoderma 156 (3–4), 75–83. https://doi.org/10.1016/j.geoderma.2010.02.003.
Queiroz, G.L., McDermid, G.J., Linke, J., Hopkinson, C., Kariyeva, J., 2020. Estimating coarse woody debris volume using image analysis and multispectral LiDAR. Forests 11 (2), 141.
Reilly, M.J., Dunn, C.J., Meigs, G.W., Spies, T.A., Kennedy, R.E., Bailey, J.D., Briggs, K., 2017. Contemporary patterns of fire extent and severity in forests of the Pacific Northwest, USA (1985 2010). Ecosphere 8 (3). https://doi.org/10.1002/ecs2.1695.
Shakesby, R.A., Doerr, S.H., 2006. Wildfire as a hydrological and geomorphological agent. Earth-Sci. Rev. 74, 269–307.
Shenoy, A., Johnstone, J.F., Kasischke, E.S., Kielland, K., 2011. Persistent effects of fire severity on early successional forests in interior Alaska. For. Ecol. Manage. 261 (3), 381–390. https://doi.org/10.1016/j.foreco.2010.10.021.
Steel, Z.L., Safford, H.D., Viers, J.H., 2015. The fire frequency-severity relationship and the legacy of fire suppression in California forests. Ecosphere 6 (1). https://doi.org/10.1890/es14-00224.1.
Stinson, G., Kurz, W.A., Smyth, C.E., Neilson, E.T., Dymond, C.C., Metsaranta, J.M., Boisvenue, C., Rampley, G.J., Li, Q., White, T.M., Blain, D., 2011. An inventory-based analysis of Canada's managed forest carbon dynamics, 1990 to 2008. Glob. Change Biol. 17 (2227), 2244.
Thompson, D.K., Wotton, B.M., Waddington, J.M., 2015. Estimating the heat transfer to an organic soil surface during crown fire. Int. J. Wildland Fire 24.
Turetsky, M.R., Benscoter, B., Page, S., Rein, G., Van Der Werf, G.R., Watts, A., 2015. Global vulnerability of peatlands to fire and carbon loss. Nat. Geosci. 1, 11–14.
Turner, M.G., Romme, W.H., Gardner, R.H., 1999. Prefire heterogeneity, fire severity, and early postfire plant reestablishment in subalpine forests of Yellowstone National Park, Wyoming. Int. J. Wildland Fire 9 (1), 21. https://doi.org/10.1071/wf99003.
Ung, C.-H., Bernier, P., Guo, X.-J., 2008. Canadian national biomass equations: new parameter estimates that include British Columbia data. Can. J. For. Res. 2008 (38), 1123–1132. https://doi.org/10.1139/X07-224.
Van der Werf, G.R., Randerson, J.T., Giglio, L, Collatz, G.J., Mu, M., Kasibhatla, P.S., Morton, D.C., DeFries, R.S., Jin, Y.V., van Leeuwen, T.T., 2010. Global fire emissions and the contribution of deforestation, savanna, forest, agricultural, and peat fires (1997–2009). Atmos. Chem. Phys. 10 (23), 11707–11735.
Verbyla, D.L., Kasischke, E.S., Hoy, E.E., 2008. Seasonal and topographic effects on estimating fire severity from Landsat TM/ETM+ data. Int. J. Wildland Fire 17 (4), 527–534.
Wang, H., Piazza, S.C., Sharp, L.A., Stagg, C.L., Couvillion, B.R., Steyer, G.D., McGinnis, T.E., 2017a. Determining the spatial variability of wetland soil bulk density, organic matter, and the conversion factor between organic matter and organic carbon across coastal Louisiana, U.S.A. J. Coastal Res. 33 (3), 507–517.
Wang, X., Parisien, M.-A., Taylor, S.W., Candau, J.-N., Stralberg, D., Marshall, G.A., Flannigan, M.D., 2017b. Projected changes in daily fire spread across Canada over the next century. Environ. Res. Lett. 12 (2), 025005 https://doi.org/10.1088/1748-9326/aa5835.
Westerling, A.L., 2016. Increasing western US forest wildfire activity: sensitivity to changes in the timing of spring. Philos. Trans. Roy. Soc. B: Biol. Sci. 371 (1696), 20150178. https://doi.org/10.1098/rstb.2015.0178.
Whitman, T., Whitman, E., Woolet, J., Flannigan, M.D., Thompson, D.K., Parisien, M.-A., 2019. Soil bacterial and fungal response to wildfires in the Canadian boreal forest across a burn severity gradient. Soil Biol. Biochem. 138, 107571 https://doi.org/10.1016/j.soilbio.2019.107571.
Whitman, E., Parisien, M.A., Thompson, D.K., Hall, R.J., Skakun, R.S., Flannigan, M.D., 2018. Variability and drivers of burn severity in the northwestern Canadian boreal forest. Ecosphere 9 (2), e02128.
Wilkinson, S.L., Moore, P.A., Flannigan, M.D., Wotton, B.M., Waddington, J.M., 2018. Did enhanced afforestation cause high severity peat burn in the Fort McMurray Horse River wildfire? Environ. Res. Lett. 13 (1), 014018.
Wotton, B.M., Flannigan, M.D., Marshall, G.A., 2017. Potential climate change impacts on fire intensity and key wildfire suppression thresholds in Canada. Environ. Res. Lett. 12 (9), 095003 https://doi.org/10.1088/1748-9326/aa7e6e.
Zehetgruber, B., Kobler, J., Dirnböck, T., Jandl, R., Seidl, R., Schindlbacher, A., 2017. Intensive ground vegetation growth mitigates the carbon loss after forest disturbance. Plant Soil 420 (1–2), 239–252. https://doi.org/10.1007/s11104-017-3384-9.
Zhou, G., Liu, S., Li, Z., Zhang, D., Tang, X., Zhou, C., Mo, J., 2006. Old-growth forests can accumulate carbon in soils. Science 314 (5804), 1417 1417. https://doi.org/10.1126/science.1130168.